



Transport and fusion of Majorana zero modes in the presence of nonadiabatic transitionsQiongyao Wang ^{1,*}, Jing Bai,^{1,*} Luting Xu,¹ Wei Feng,^{1,†} and Xin-Qi Li^{1,2,‡}¹*Center for Joint Quantum Studies and Department of Physics, School of Science, Tianjin University, Tianjin 300072, China*²*Center for Quantum Physics and Technologies, School of Physical Science and Technology, Inner Mongolia University, Hohhot 010021, China* (Received 2 March 2024; revised 15 July 2024; accepted 13 August 2024; published 3 September 2024)

We perform simulations for transport and nontrivial fusion of Majorana zero modes in topological superconducting quantum wires. We uncover interesting behaviors of nonadiabatic transition associated with the transport through mini-gate-controlled multiple-segment modulations. Owing to breaking of the initial fermion parity induced by nonadiabatic transitions, a deviation from the statistics of outcomes of nontrivial fusion arises and is analyzed. Moreover, we develop a measurement scheme to infer the amount of fermion parity breaking and nonadiabatic transition probability to excited states, based on the characteristic spectrum of measurement current by a quantum-point-contact detector, by measurement of the charge occupation dynamics in a fusion-outcome-probing quantum dot.

DOI: [10.1103/PhysRevB.110.115402](https://doi.org/10.1103/PhysRevB.110.115402)**I. INTRODUCTION**

The nonlocal property of the Majorana zero modes (MZMs) and the non-Abelian statistics obeyed by them provide the foundation for application to topological quantum computation [1–6]. The nature of the non-Abelian statistics of the MZMs indicates that braiding the MZMs can result in quantum state evolution in the manifold of highly degenerate ground states [7–11]. The non-Abelian nature of MZMs also indicates that fusing a pair of MZMs can yield an outcome of either a vacuum or an unpaired fermion (resulting in an extra charge) [12–18]. In the literature, this is usually termed *nontrivial* fusion. These braiding and fusing behaviors are closely related to each other. In one aspect (the fundamental aspect), the fusion with two outcomes can serve as a demonstration of non-Abelian statistics since it indicates the quantum dimension $d > 1$ (a degeneracy of the ground state manifold), which leads to, after braiding the MZMs, a unitary evolution matrix acting on the degenerate ground state manifold, rather than to a scalar phase factor on a single nondegenerate state. In the other aspect, even computationally speaking, braiding is not needed if one can fuse arbitrary sets of 2 and 4 zero modes [13].

In practice, typically, both braiding and fusion require moving/transporting the MZMs in real space. For instance, for braiding operations, the early and representative scheme is quantum-adiabatically moving the MZMs by tuning a series of electric gates to drive different regions of the Majorana quantum wire into the topological or nontopological regime [7,8,19,20]. This scheme is motivated by the fact that the

MZMs will form at the boundaries between the topological and nontopological regions. With the progress of gating control techniques, the Majorana moving schemes have gained renewed interests in the past few years [9,10,21–23]. For fusion, as recently proposed in Ref. [14] and further analyzed in Ref. [15], nontrivial fusion of MZMs can be demonstrated by fusing a pair of MZMs from two topological superconducting (TSC) wires (each wire accommodating two MZMs at the ends). To demonstrate the most interesting case of nontrivial fusion, it is required to prepare the initial pair states of MZMs with definite fermion parities and nonadiabatically move the MZMs together to fuse, as shown schematically in Fig. 1(a).

For both braiding and fusion, to keep up the topological protection, the quantum transport of MZMs should be adiabatically slow. However, this may contradict other requirements, such as avoiding the quasiparticle-poisoning decoherence. Thus, the effect of nonadiabatic transition constitutes an important subject in the Majorana community [21,22,24–30]. Moreover, how to experimentally measure out the nonadiabatic transition is another related important and interesting problem. This has been addressed in an initial study in Ref. [31], where a transport probe scheme (in terms of tunneling spectroscopy of Majorana conductances) was analyzed.

In this paper, following Ref. [14] and going drastically beyond Ref. [15], we perform simulations based on the lattice model of Rashba TSC quantum wires for the transport and fusion of MZMs, starting with the initial state of definite fermion parity (e.g., even parity). Notice that, in Ref. [15], the effective low-energy MZMs were directly used to analyze the fusion and probing dynamics; thus, the nonadiabatic effects caused by the moving and their consequence to the result of fusion and probing dynamics cannot be accounted for. Specifically, in this paper, considering the progress of the mini-gate-control technique, we simulate the gradual

*These authors equally contributed to this work.

†Contact author: fwphy@tju.edu.cn

‡Contact author: xinqi.li@imu.edu.cn

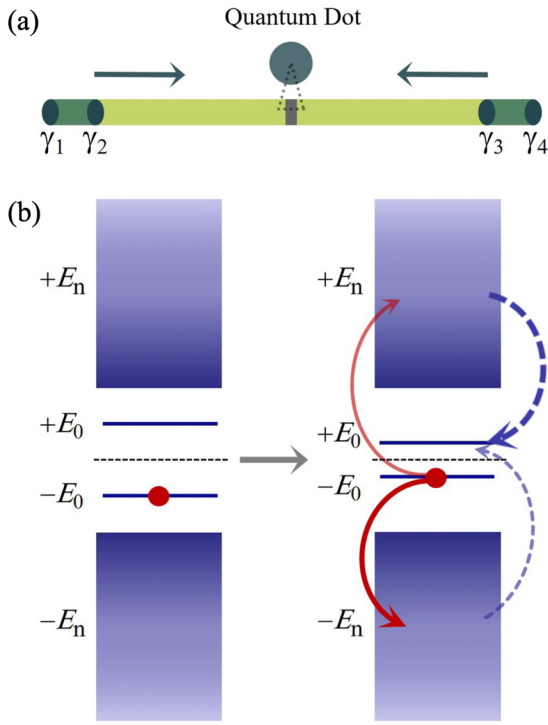


FIG. 1. (a) Schematic diagram of mini-gate-controlled transport of Majorana zero modes (MZMs) and nontrivial fusion of a pair of MZMs, say, γ_2 and γ_3 , from different Majorana pairs with definite fermion parities (e.g., even parity) prepared in advance. Based on the fusion rule $\gamma_2 \times \gamma_3 = I + \psi$, the fused MZMs would yield probabilistic outcomes of vacuum I and a regular fermion ψ . A quantum dot (QD) is introduced to couple to the fused MZMs for probing the fusion outcomes, while the charge fluctuations in the QD can be detected by a nearby quantum-point-contact device (not shown in this plot). (b) Bogoliubov–de Gennes (BdG) energy diagram of a TSC quantum wire (taking one of the two wires shown here as an example, and omitting the labels L and R for the left and right wires). The transport of the MZM is assumed to start with the even parity state $|0\rangle$, which is described by occupation of the negative energy state $|\psi_{-E_0}\rangle$, as shown in the left panel. In the right panel, a possible nonadiabatic transition during moving the MZM is conceptually illustrated.

transport of MZMs by modulation of multiple segments from nontopological to topological transitions and uncover interesting behaviors of nonadiabatic transition associated with this type of modulation. Being of great interest, owing to partly (weakly) switching to an opposite-parity zero-energy state, which is mediated by the nonadiabatic transition to high-energy excited states, we notice that the initial fermion parity will be broken by some amount. Accordingly, the result will suffer some deviation from the statistics of outcomes of nontrivial fusion. Following Refs. [14,15], by considering the use of a quantum-point-contact (QPC) detector and a quantum dot (QD) to probe the outcomes of nontrivial fusion, very importantly, we will develop a scheme to infer simultaneously both the degree of fermion parity breaking and nonadiabatic transition probability to excited states, based on the characteristic spectrum of QPC measurement current. The proposed scheme of probing either the intrinsic fermion-parity

breaking of MZMs or their nonadiabatic transition probability to excited states should be of great interest to the Majorana community, considering that this type of study is lacking in the literature, to the best of our knowledge.

II. MODEL AND THE BOGOLIUBOV-DE GENNES FORMULATION

For the various realizations based on proximitized semiconductor/superconductor (SM/SC) hybrid structure, the TSC quantum wire can be described by a discretized lattice model as follows [21]:

$$\begin{aligned}
 H_{\text{QW}} = & -\frac{W}{2} \sum_{i\sigma} (c_{i,\sigma}^\dagger c_{i+1,\sigma} + c_{i+1,\sigma}^\dagger c_{i,\sigma}) \\
 & + (W - \mu) \sum_{i\sigma} c_{i,\sigma}^\dagger c_{i,\sigma} + V_z \sum_{i\sigma\sigma'} c_{i,\sigma}^\dagger (\sigma^z)_{\sigma\sigma'} c_{i,\sigma'} \\
 & + \frac{\alpha_{\text{SO}}}{2} \sum_{i\sigma\sigma'} [c_{i,\sigma}^\dagger (i\sigma^y)_{\sigma\sigma'} c_{i+1,\sigma'} + c_{i+1,\sigma'}^\dagger (i\sigma^y)_{\sigma\sigma'} c_{i,\sigma}] \\
 & + \Delta \sum_{i\sigma} (c_{i,\uparrow} c_{i,\downarrow} + c_{i,\downarrow}^\dagger c_{i,\uparrow}^\dagger). \quad (1)
 \end{aligned}$$

Following Ref. [21], in the simulations of this paper, we choose the wire parameters (in a reduced arbitrary system of units) as the hopping energy $W = 1$, the superconducting gap $\Delta = 0.3$, the Zeeman energy $V_z = 0.4$, the spin-orbit-interaction (SOI) strength $\alpha_{\text{SO}} = 0.3$, and the chemical potentials $\mu = \mu_{\text{T}} = 0$ and $\mu = \mu_{\text{nT}} = -0.45$ for the topological and nontopological regimes.

For the purpose of numerical simulation of moving the MZMs within the Bogoliubov–de Gennes (BdG) formalism, the BdG Hamiltonian matrix H_{BdG} can be obtained through the following identity:

$$H_{\text{QW}} = \frac{1}{2} \hat{\Psi}^\dagger H_{\text{BdG}} \hat{\Psi}, \quad (2)$$

where $\hat{\Psi} = (c_{1\uparrow} \cdots c_{N\uparrow}, c_{1\downarrow} \cdots c_{N\downarrow}, c_{1\uparrow}^\dagger \cdots c_{N\uparrow}^\dagger, c_{1\downarrow}^\dagger \cdots c_{N\downarrow}^\dagger)^T$ is the so-called Nambu spinor. The BdG Hamiltonian matrix H_{BdG} can be also understood as being constructed under the basis of electron and hole states of the lattice sites, i.e., $\{|e_{j\sigma}\rangle, |h_{j\sigma}\rangle; j = 1, 2, \dots, N\}$. Accordingly, the wave function of the TSC wire can be expressed as $|\Psi(t)\rangle = \sum_{j,\sigma} (u_{j\sigma}(t)|e_{j\sigma}\rangle + v_{j\sigma}(t)|h_{j\sigma}\rangle)$, which is the solution of the time-dependent BdG (TDBdG) equation $i\partial_t |\Psi\rangle = H_{\text{BdG}} |\Psi\rangle$. To identify the low-energy states (from which the MZMs are defined) and nonadiabatic transitions to the excited Bogoliubov quasiparticle states, it is useful to recast the wire state as

$$|\Psi(t)\rangle = \alpha_0 |\psi_{-E_0}\rangle + \beta_0 |\psi_{+E_0}\rangle + \sum_{n \neq 0} (\alpha_n |\psi_{-E_n}\rangle + \beta_n |\psi_{+E_n}\rangle), \quad (3)$$

in which the instantaneous eigenstates are obtained through $H_{\text{BdG}}(t) |\psi_{\pm E_n}(t)\rangle = \pm E_n(t) |\psi_{\pm E_n}(t)\rangle$. In the BdG formalism, the negative energy state $|\psi_{-E_n}\rangle$ is the charge-conjugated counterpart of the positive energy state $|\psi_{+E_n}\rangle$, holding the particle and antiparticle corresponding relation.

As schematically shown in Fig. 1(a), we will consider the transport and fusion of the Majorana modes γ_2 and γ_3 , with an aim at demonstrating the nontrivial fusion rule

$\gamma_2 \times \gamma_3 = I + \psi$. This rule implies that the fused MZMs would yield a probabilistic outcome of the vacuum I or a regular fermion ψ . For this purpose, γ_2 and γ_3 should come from different Majorana pairs with definite fermion parities. To be specific, the above nontrivial fusion rule can be examined through the following state transformation [12,14]:

$$|0_{12}0_{34}\rangle = \frac{1}{\sqrt{2}}(|0_{23}0_{14}\rangle + i|1_{23}1_{14}\rangle). \quad (4)$$

Here, the regular fermion number states $|n_{12}n_{34}\rangle$ and $|n_{23}n_{14}\rangle$ are defined through different combinations of the four Majorana modes. For instance, n_{12} is the particle number of the regular fermion f_{12} , associated with the Majorana modes γ_1 and γ_2 . Other particle number states are defined in the same way. Therefore, in practice, we need to prepare the initial state $|0_{12}0_{34}\rangle$ and adiabatically move the Majorana modes γ_2 and γ_3 together to fuse. According to the proposal in Ref. [14], this can be realized as follows. By means of mini-gate-voltage control, first, move γ_2 and γ_3 to the ends of the two wires, close to γ_1 and γ_4 , respectively; then empty the possible occupations of the regular fermions f_{12} and f_{34} by introducing tunnel-coupled side QDs and modulating the dot energies (while the QDs are also tunnel coupled to outside reservoirs). Starting with $|0_{12}0_{34}\rangle$, move γ_2 and γ_3 from the two terminal sides back to the central part to fuse such that $\epsilon_M \neq 0$. In the basis of n_{12} and n_{34} occupations, the fused state is still $|0_{12}0_{34}\rangle$, but in the basis of n_{23} and n_{14} occupations, two possible outcomes with $n_{23} = 0$ or 1 will be generated, as shown above in Eq. (4).

Following Refs. [11,14], starting with $|0_{12}0_{34}\rangle$ but to simulate the possible nonadiabatic transitions, we need to convert the description from the occupation number states to the BdG positive and negative energy states. We thus consider simulating moving the MZMs γ_2 and γ_3 with the initial state $|\psi_{-E_0^L}, \psi_{-E_0^R}\rangle$. This is actually the *dual counterpart* of starting with $|1_{12}1_{34}\rangle$, which should be converted into the initial state $|\psi_{+E_0^L}, \psi_{+E_0^R}\rangle$, for the sake of moving the simulation within the BdG framework. Here, we introduced the superscripts L and R to denote the left and right TSC wires.

III. MAJORANA TRANSPORT AND NONADIABATIC TRANSITION

The transport of MZMs can be realized via the control of mini-gates as proposed in Ref. [14], i.e., sequentially changing the chemical potentials of segments of the quantum wire, to realize transitions from the nontopological to the topological regime. Specifically, we assume the modulation of the chemical potential $\mu_j(t)$ of the j th segment occurs according to $\mu_j(t) = \{1 - f[(t - t_j)/\tau]\}\mu_{nT} + f[(t - t_j)/\tau]\mu_T$, with $f(s)$ a monotonically increasing function and satisfying $f(0) = 0$ and $f(1) = 1$. Following Ref. [21], we assume $f(s) = \sin^2(s\pi/2)$. For an m -segment modulation scheme with total time T , the time of moving through each segment is $\tau = t_{j+1} - t_j = T/m \equiv T_m$. In this paper, we consider the following interesting problem: For the same T , what is the difference of nonadiabatic transition between different choices of m and T_m ? This type of information should be useful for experiments along this line.

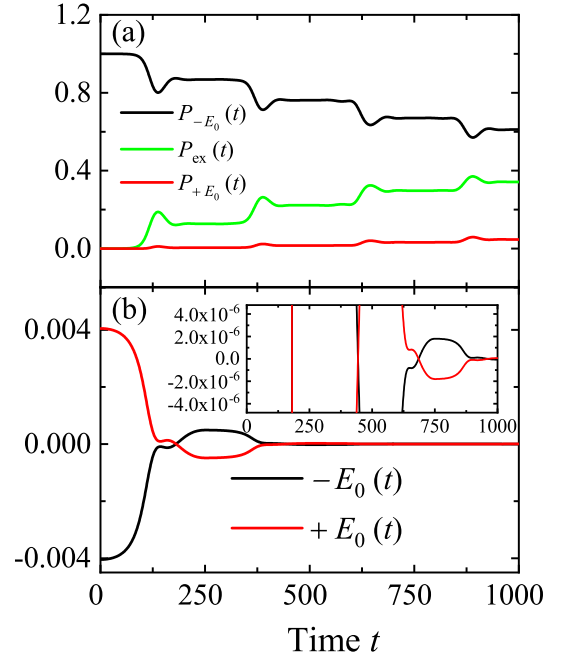


FIG. 2. Taking the 4-segment mini-gate-controlled moving sequence as an example, (a) the dynamical evolution of the occupation probabilities of the negative eigenstate $|\psi_{-E_0}(t)\rangle$, the positive eigenstate $|\psi_{+E_0}(t)\rangle$, and all the excited states; and (b) the energy diagram of the instantaneous eigenstates $|\psi_{-E_0}(t)\rangle$ and $|\psi_{+E_0}(t)\rangle$. The inset in (b) is the same result as in the main figure, only using a smaller range of vertical coordinate to enlarge the visual effect. To determine $P_{-E_0}(t)$ and $P_{+E_0}(t)$, it is necessary to properly track the evolution of $|\psi_{-E_0}(t)\rangle$ and $|\psi_{+E_0}(t)\rangle$ in the presence of Majorana energy oscillations (positive and negative energy crossings). Parameters of the topological superconducting (TSC) quantum wire used in the simulation are referred to the main text below Eq. (1).

In Fig. 2, we first display the basic behavior of a nonadiabatic transition associated with the multiple-segment modulation for moving the MZM in a single wire. To be specific, we consider a quantum wire with $N = 50$ lattice sites and the modulation segment number $m = 4$, with thus each segment having 10 lattice sites. In this paper, we always consider moving the MZM in the wire from a side topological segment with 10 lattice sites, as schematically shown in Fig. 1(a). In Fig. 2(a), we illustrate the dynamical evolution of $P_{-E_0}(t)$, $P_{+E_0}(t)$, and $P_{ex}(t)$, which are, respectively, the occupation probabilities of the initial state $|\psi_{-E_0}\rangle$, the positive-lowest-energy state $|\psi_{+E_0}\rangle$, and all excited states. Here, $P_{ex}(t)$ is simply defined through $P_{ex}(t) = \sum_{n \neq 0} [|\alpha_n(t)|^2 + |\beta_n(t)|^2]$ from Eq. (3) or, equivalently, through $P_{ex}(t) = 1 - [P_{-E_0}(t) + P_{+E_0}(t)]$. Without loss of generality, here, we consider moving a MZM in a single wire, thus omitting the superscripts L and R (which have been introduced to denote the left and right wires). We find that, when moving the MZM through each segment, via gate-voltage control, a nonadiabatic transition takes place, which reduces $P_{-E_0}(t)$ and increases $P_{ex}(t)$ and $P_{+E_0}(t)$. In this context, we may first remark that the nonadiabatic transition to the same type of BdG state, i.e., the type of positive and negative energy states, is for the same reason of nonadiabatic transition governed by quantum mechanics. However, the nonadiabatic

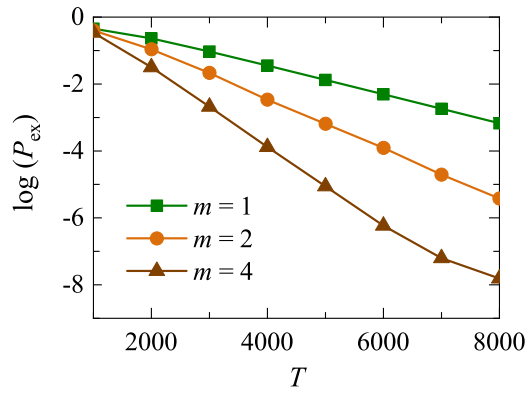


FIG. 3. Nonadiabatic transition probabilities to excited states $P_{\text{ex}} = 1 - (P_{-E_0} + P_{+E_0})$ vs the total moving time T for different- m -segment moving schemes, with m defined as $T = mT_m$. Parameters of the topological superconducting (TSC) quantum wire are given in the main text below Eq. (1).

transition to the different types of states involves the splitting or formation of a Cooper pair and is possible owing to the existence of a large number of unpaired normal electrons in the SC.

Then let us discuss the results of Fig. 2(a) in more detail. The dip and peak behaviors of $P_{-E_0}(t)$ and $P_{\text{ex}}(t)$ are owing to the closing of the superconducting gap, during crossing from the nontopological to the topological regime, thus suffering a relatively stronger nonadiabatic transition. We also notice that the probability $P_{+E_0}(t)$ is much smaller than $P_{\text{ex}}(t)$. This seemingly contradicts the *adiabatic condition* in quantum mechanics since the energy difference of $|\psi_{+E_0}\rangle$ from $|\psi_{-E_0}\rangle$ is much smaller than the excited quasiparticle states from $|\psi_{-E_0}\rangle$. We may understand this important point as follows. In Ref. [11], it was pointed out that the particle-hole symmetry would prohibit *direct transition* between the particle-hole symmetric eigenstates, i.e., $\Pi_{+E_n, -E_n} = i\langle\psi_{+E_n}(\mathbf{R})|\partial_t[\psi_{-E_n}(\mathbf{R})]\rangle = 0$, while the Berry connection matrix is defined more generally as $\Pi_{\pm E_n, \pm E_m} = i\langle\psi_{\pm E_n}(\mathbf{R})|\partial_t[\psi_{\pm E_m}(\mathbf{R})]\rangle$, with \mathbf{R} denoting the time-dependent system parameters. Then we know that there is no direct nonadiabatic transition coupling between $|\psi_{+E_0}\rangle$ and $|\psi_{-E_0}\rangle$. The appearance of nonzero small $P_{+E_0}(t)$ is thus caused by an *indirect* nonadiabatic transition process, i.e., from $|\psi_{-E_0}\rangle$ to $|\psi_{+E_0}\rangle$ mediated by the excited quasiparticle states.

We may remark that, to determine $P_{-E_0}(t)$ and $P_{+E_0}(t)$, it is necessary to track the time-dependent evolution of the states $|\psi_{-E_0}\rangle$ and $|\psi_{+E_0}\rangle$. In Fig. 2(b), we display the eigenenergies of these two states. We find that the positive and negative energies interchange after passing through a crossing point when the MZM moves through each segment. This is the so-called *Majorana oscillation* phenomenon [32–34], owing to the fact that, in realistic finite-length quantum wires, the Majorana modes hybridize and the hybridization energy oscillates as a function of the Zeeman energy, chemical potential, or wire length. Properly addressing this issue is essential to obtain the results in Fig. 2(a); otherwise, sudden jumps of occupation would be wrongly obtained.

In Fig. 3, we display the nonadiabatic transition probability to excited states $P_{\text{ex}}(T)$ for its T (total moving time) dependence. This qualitatively corresponds to the Landau-Zener

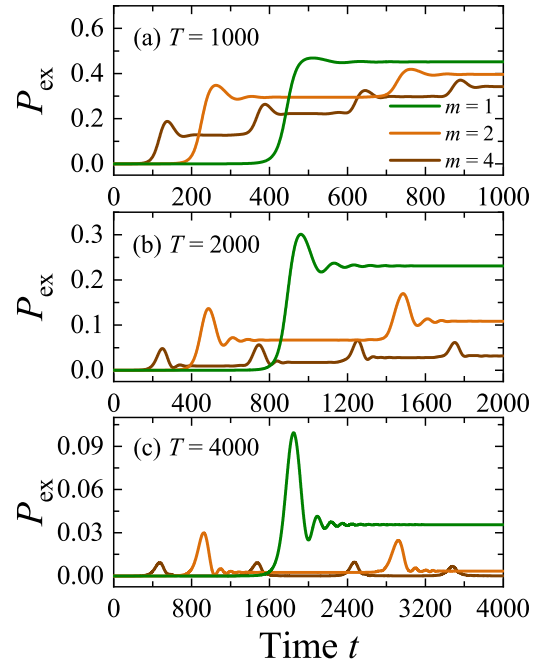


FIG. 4. Additional insight into the results shown in Fig. 3, from the transient behaviors of the nonadiabatic transition probabilities of different m -segment moving schemes, with m defined as $T = mT_m$, while T is the total moving time, as exemplified by setting (a) $T = 1000$, (b) $T = 2000$, and (c) $T = 4000$. Indeed, weaker nonadiabatic transition is found for moving through more mini-gate-controlled segments (larger m) but with the same total time T . Parameters of the topological superconducting (TSC) quantum wire are given in the main text below Eq. (1).

tunneling behavior, with an increase of T , say, causing the nonadiabatic transition to become weaker. Here, we compare the results of three different transport schemes, which are specified by $m = 1, 2$, and 4 for, respectively, the 1-, 2-, and 4-segment transport schemes. Interestingly, we find that the nonadiabatic transition is weaker for the transport by means of multiple-segment modulation.

In Fig. 4, taking a few different values of T as examples, we detail what happens in the moving process for each moving scheme. We see that, for the one-step moving, strong nonadiabatic transition occurs around the superconducting-gap-closing place, while for the multiple-segment moving scheme, multiple nonadiabatic transitions take place near the gap-closing points in moving through each segment, as observed in the $m = 2$ and 4 curves. However, the summed probability of the multiple nonadiabatic transitions becomes smaller with the increase of the segment numbers of mini-gate control. This may partly explain the reason for the results in Fig. 3.

We may mention that our above result is only from limited numerical simulations (for small number of segments). The above result is basically consistent with that revealed in Ref. [30], where the transport of MZMs was simulated using the Kitaev chain model and analyzed by a generalized Landau-Zener transition formula. In Ref. [30], it was concluded that, to reduce nonadiabatic transition, there exists an optimized choice of m for the multiple-segment control of MZM transport. However, as shown in Ref. [21], the Rashba

TSC quantum wire is more complicated, and the nonadiabatic transition in the Rashba TSC quantum wire does not agree well with the Landau-Zener transition formula. Whether or not the conclusion of Ref. [30] is valid for the Rashba TSC quantum wire seems an open question, which needs further systematic studies.

We may also mention that our results of the manipulation time T dependence display a large range of nonadiabatic transition behaviors. However, the range of T we simulated corresponds to moving velocities below the critical velocity v_c determined from the inequality of adiabatic condition, as given by eqs. (38) and (43) in Ref. [26]. Qualitatively speaking, after violating that condition, the nonadiabatic transition effect will be obvious. However, such an *inequality condition* (which is used to define the critical velocity v_c) does not mean something like the sharp condition (critical point) in *phase transition* phenomena. Below v_c , there exists also a considerable nonadiabatic transition. We also noticed that, in Ref. [27], it was concluded that, when the domain-wall moving velocity is larger than the *effective* light speed (like the critical velocity v_c), i.e., the Majorana mode is in superluminal motion, the Majorana mode will become unstable, say, with a transition taking place from a localized to an extended state. However, this remarkable result likely needs more careful and serious examinations, especially by numerical simulations using various non-Dirac types of electron models.

IV. FERMION PARITY BREAKING AND ITS CONSEQUENCE

After moving the MZMs γ_2 and γ_3 to the central part (before fusing and coupling to the probing QD), the nonadiabatic transition analyzed above would render the states of the left and right wires as $|\Psi_\mu(t)\rangle = \alpha_\mu|\psi_{-E_0^\mu}\rangle + \beta_\mu|\psi_{+E_0^\mu}\rangle + (\dots)$. Here, μ denotes L and R, and (\dots) stands for the components of excited states. Noting that Majorana fusion and probe coupling to the QD are dominantly taking place within the subspace of low-energy states, the high-energy excited states will be gapped out in the fusing and probing process. Then the wire state after moving can be expressed as

$$|\Psi_{LR}(0)\rangle = (\alpha_L|0_{12}\rangle + \beta_L|1_{12}\rangle) \otimes (\alpha_R|0_{34}\rangle + \beta_R|1_{34}\rangle). \quad (5)$$

Here, the states of MZMs have been converted to the number states of regular fermion occupation. This product state has four components. Indeed, the fusion rule of Eq. (4) accounts for the most interesting case from the state $|0_{12}0_{34}\rangle$.

However, as pointed out in Ref. [13], nontrivial fusion can be reasonable for any initial state with definite parity. Therefore, we carry out the following transformation rules [15]:

$$\begin{aligned} |1_{12}1_{34}\rangle &= \frac{1}{\sqrt{2}}(|0_{14}0_{23}\rangle - i|1_{14}1_{23}\rangle), \\ |0_{12}1_{34}\rangle &= \frac{1}{\sqrt{2}}(|1_{14}0_{23}\rangle + i|0_{14}1_{23}\rangle), \\ |1_{12}0_{34}\rangle &= \frac{1}{\sqrt{2}}(|1_{14}0_{23}\rangle - i|0_{14}1_{23}\rangle). \end{aligned} \quad (6)$$

Based on Eqs. (4) and (6), one can check that the average of the parity $P_{23} = i\gamma_2\gamma_3$ is zero for any of the four states. That

is, for any (initial) state $|n_{12}n_{34}\rangle$ with definite parity, the fusion of γ_2 and γ_3 will result in the statistical average $\langle P_{23} \rangle = 0$, as formally proved in Ref. [13]. This result reflects the key feature of nontrivial fusion with equal weight outcomes of I and ψ .

Accordingly, let us consider the statistical average of P_{23} over the wire state $|\Psi_{LR}(0)\rangle$, given by Eq. (5). Let us reexpress this state in the basis $\{|n_{14}n_{23}\rangle\}$. Simple algebra yields

$$\begin{aligned} |\Psi_{LR}(0)\rangle &= \frac{1}{\sqrt{2}}(A_+|0_{14}\rangle + B_+|1_{14}\rangle)|0_{23}\rangle \\ &\quad + \frac{i}{\sqrt{2}}(A_-|1_{14}\rangle + B_-|0_{14}\rangle)|1_{23}\rangle. \end{aligned} \quad (7)$$

Here, we introduced $A_\pm = \alpha_L\alpha_R \pm \beta_L\beta_R$ and $B_\pm = \alpha_L\beta_R \pm \beta_L\alpha_R$. If we only consider the fusion of γ_2 and γ_3 (but not coupling to the QD), the fusion just removes the energy degeneracy between $|0_{23}\rangle$ and $|1_{23}\rangle$ but renders the above state unchanged, except a phase factor $\exp(-i\epsilon_M t)$ attached to $|1_{23}\rangle$ (with ϵ_M the coupling energy of γ_2 and γ_3). This observation indicates that $\langle P_{23} \rangle$ is the same before and after the fusion of γ_2 and γ_3 :

$$\begin{aligned} \langle P_{23} \rangle &= -\frac{1}{2}(|A_+|^2 + |B_+|^2) + \frac{1}{2}(|A_-|^2 + |B_-|^2) \\ &= -2 \operatorname{Re}[(\alpha_L\alpha_R)^*(\beta_L\beta_R) + (\alpha_L\beta_R)^*(\beta_L\alpha_R)]. \end{aligned} \quad (8)$$

From this result, we see that nonzero $\langle P_{23} \rangle$ is caused by the *nonadiabatic-transition-induced* mixing of $|1_{12}\rangle$ and $|1_{34}\rangle$ into the initially prepared left and right wire states $|0_{12}\rangle$ and $|0_{34}\rangle$, thus violating the definite parity condition of each wire. In other words, the nonadiabatic transition would induce a breaking of the initial fermion parity associated with the MZMs. Furthermore, the result of nonzero $\langle P_{23} \rangle$ is caused by the interference among the 4-MZMs states, between the two even-parity states, and between the two odd-parity states. In Fig. 5, we numerically demonstrate the effect of the fermion parity breaking caused by nonadiabatic transition, by plotting the nonzero $\langle P_{23} \rangle$, together with the probabilities of remaining in the initial state and going to the opposite parity state. As will become clear in the following, this mechanism of leading to $\langle P_{23} \rangle \neq 0$ can be inferred through a careful analysis for the QD occupation dynamics.

V. PROBING DYNAMICS AND INFORMATION EXTRACTION

Following Ref. [14], let us couple a nearby QD (with a single energy level ϵ_D) to the fused MZMs γ_2 and γ_3 , with coupling amplitudes λ_2 and λ_3 . In the picture of the regular fermion f_{23} , the coupling Hamiltonian reads as

$$H' = (\lambda_N d^\dagger f_{23} + \lambda_A d^\dagger f_{23}^\dagger) + \text{H.c.}, \quad (9)$$

where d^\dagger is the creation operator of the QD electron. Physically, the first term describes the usual normal tunneling process, and the second term describes the Andreev process owing to Cooper pair splitting and recombination. The respective coupling amplitudes are associated with λ_2 and λ_3 as $\lambda_{N,A} = \lambda_2 \pm i\lambda_3$. We assume that the QD is initially prepared in an empty state $|0_d\rangle$, and the probe-coupling-caused state

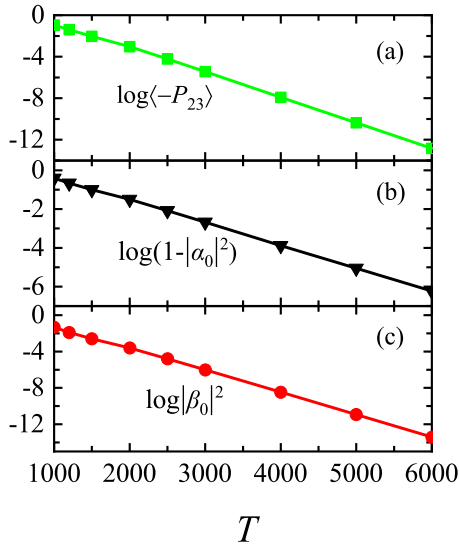


FIG. 5. Breaking of the initial fermion parity caused by nonadiabatic transition. (a) Degree of $\langle P_{23} \rangle \neq 0$ vs the moving time, indicating a violation of the statistics of nontrivial fusion outcomes, with definite initial parity, which requires $\langle P_{23} \rangle = 0$ [13]. (b) and (c) Associated probabilities of remaining in the initial state and going to the opposite parity state, after moving the Majorana zero mode (MZM) in a single wire. In essence, $\langle P_{23} \rangle \neq 0$ is a consequence of quantum interference between the two different parity states (see the main text for details). Parameters of the topological superconducting (TSC) quantum wire are given in the main text below Eq. (1).

evolution is described as

$$\begin{aligned} U_c(t)|0_{23}0_d\rangle &= \alpha_A(t)|0_{23}0_d\rangle + \beta_A(t)|1_{23}1_d\rangle, \\ U_c(t)|1_{23}0_d\rangle &= \alpha_N(t)|1_{23}0_d\rangle + \beta_N(t)|0_{23}1_d\rangle, \end{aligned} \quad (10)$$

where $U_c(t)$ is the coupling-caused evolution operator. Let us denote $|\Psi_{\text{tot}}(t)\rangle = U_c(t)[|\Psi_{\text{LR}}(0)\rangle \otimes |0_d\rangle]$. The QD occupation is then obtained as

$$\begin{aligned} P_d(t) &= \langle \Psi_{\text{tot}}(t) | d^\dagger d | \Psi_{\text{tot}}(t) \rangle \\ &= \frac{1}{2} [|\beta_A(t)|^2 M_A + |\beta_N(t)|^2 M_N]. \end{aligned} \quad (11)$$

Here, $M_{A,N} = |A_\pm|^2 + |B_\pm|^2$, playing the role of *modification* to the result of the ideal case (in the absence of nonadiabatic transition), i.e., $P_d(t) = \frac{1}{2} (|\beta_A|^2 + |\beta_N|^2)$. Also, after a simple derivation, we obtain the charge transfer probabilities into the QD through the two channels (associated with the two fusion outcomes), as

$$|\beta_{N,A}(t)|^2 = R_{N,A} \sin^2(\Omega_{N,A} t). \quad (12)$$

Here, we have defined $R_{N,A} \equiv |\lambda_{N,A}|^2 / \Omega_{N,A}^2$, while $\Omega_{N,A} = \sqrt{\Delta_{N,A}^2 + |\lambda_{N,A}|^2}$ (with $\Delta_{N,A} = |\epsilon_D \mp \epsilon_M|/2$) are the charge oscillation frequencies through the two channels.

Following Refs. [14,15], we consider monitoring the charge occupation of the QD by a QPC detector. We consider performing continuous weak measurement to extract the dynamical information of charge occupation in the QD from the output current power spectrum $S_I(\omega)$. As shown in Refs. [35–38], the structure of the current power spectrum is $S_I(\omega) = S_0 + S_d(\omega)$, where S_0 is the frequency-free

background noise, and $S_d(\omega)$ is the information-contained part. More specifically, $S_d(\omega)$ is the Fourier transformation of the correlation function $S_d(\tau)$ of the dot occupation ($n_d = d^\dagger d$):

$$S_d(\tau) = \text{Tr}[n_d e^{\mathcal{L}|\tau|} (n_d \rho_{\text{st}})]. \quad (13)$$

Here, as usual, we consider the current power spectrum of steady state ρ_{st} . The steady state is defined by the stationary solution of the master equation $\dot{\rho} = -i[H, \rho] + \kappa \mathcal{D}[n_d]\rho \equiv \mathcal{L}\rho$, where the Lindblad superoperator is defined as $\mathcal{D}[x]\rho = x\rho_c x^\dagger - \frac{1}{2}\{x^\dagger x, \rho_c\}$, and κ is the QPC measurement rate.

For each channel of charge oscillations associated with I or ψ (i.e., $n_{23} = 0$ or 1), under the condition of weak-coupling measurement, one can obtain the individual spectrum as [15,35–38]

$$\begin{aligned} S_d^{(j)}(\omega) &\simeq \frac{\Delta_j^2}{4\Omega_j^2} \frac{\kappa R_j/2}{\omega^2 + (\kappa R_j/2)^2} \\ &+ \frac{|\lambda_j|^2}{8\Omega_j^2} \frac{\frac{\kappa}{2}(1 - \frac{R_j}{2})}{(\omega - 2\Omega_j)^2 + [\frac{\kappa}{2}(1 - \frac{R_j}{2})]^2}. \end{aligned} \quad (14)$$

Here, we use $j = N, A$ to denote the two charge transfer channels, say, the normal tunneling and Andreev process. From Eq. (11), we know that the two channels are independent of each other. We thus expect the total spectrum to be a weighted sum of the individual $S_d^{(N)}(\omega)$ and $S_d^{(A)}(\omega)$, as follows:

$$S_d(\omega) = \frac{1}{2} [M_N S_d^{(N)}(\omega) + M_A S_d^{(A)}(\omega)]. \quad (15)$$

Indeed, as shown in Fig. 6, full agreement is demonstrated between this analytic result [together with Eq. (14)] and the numerical result from computation using the full states, Eqs. (7) and (10), and the master-equation-based Eq. (13).

From Eqs. (14) and (15), as shown in Fig. 6, we know that, in $S_d(\omega)$, two characteristic peaks will appear at $\omega = 2\Omega_N$ and $2\Omega_A$. The heights of the two peaks are given by $h_N = M_N h_N^{(0)}/2$ and $h_A = M_A h_A^{(0)}/2$, while $h_N^{(0)}$ and $h_A^{(0)}$ are, based on Eq. (14), known as

$$h_j^{(0)} = \frac{1}{4\kappa} \frac{R_j}{1 - R_j/2}. \quad (16)$$

Then one can extract the *modification factors* from the heights of the peaks through $M_N = 2h_N/h_N^{(0)}$ and $M_A = 2h_A/h_A^{(0)}$. Very importantly, one can check the following relation:

$$M_N - M_A = 2\langle P_{23} \rangle. \quad (17)$$

This indicates that we can infer the deviation from the statistics of outcomes of nontrivial fusion in the ideal case, which requires $\langle P_{23} \rangle = 0$. Also, in the symmetric case, say, $|\alpha_L| = |\alpha_R| = |\alpha_0|$ and $|\beta_L| = |\beta_R| = |\beta_0|$, we find another important relation:

$$M_N + M_A = 2(|\alpha_0|^2 + |\beta_0|^2)^2. \quad (18)$$

From it, one can infer the nonadiabatic transition probability to excited states in each wire, i.e., $P_{\text{ex}} = 1 - (|\alpha_0|^2 + |\beta_0|^2)$.

In practice, rather than measuring the various parameters to determine $h_N^{(0)}$ and $h_A^{(0)}$ according to Eq. (16), one can obtain them in a more practical manner as follows. As initializing the empty occupation $n_{12} = 0$ and $n_{34} = 0$ of the regular

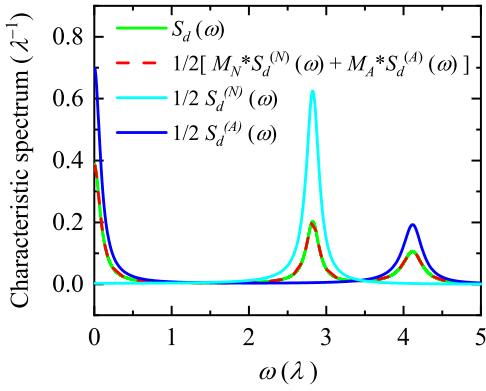


FIG. 6. The characteristic spectrum $S_d(\omega)$, the Fourier transform of the quantum dot (QD)-occupation correlation function, singled out from the quantum-point-contact (QPC) output current spectrum of continuous weak measurement. The exact numerical result (solid green line) is compared with the theoretically approximated result (dashed red line) based on Eqs. (14) and (15), and perfect agreement is demonstrated. From the location of the two peaks, one obtains the characteristic frequencies Ω_N and Ω_A of charge oscillations associated with the fusion outcomes ψ and I . Importantly, as analyzed in detail in the main text, from the heights of the two peaks, one can infer the degree of breaking of the initial fermion parity (definite parity) caused by nonadiabatic transitions, which is characterized by a nonzero $\langle P_{23} \rangle$, and infer the probability P_{ex} of nonadiabatic transition to all the excited states. In addition to the parameters of the topological superconducting (TSC) quantum wire given below Eq. (1), the numerical results shown in this plot are from a choice of other reduced parameters as $\lambda_2 = \lambda_3 = \lambda$, $\epsilon_D = \epsilon_M = 1.5\lambda$, and $\kappa = 0.4\lambda$. Notice that, to guarantee only the subgap low-energy-states involving the charge transfer dynamics, the condition $\lambda \ll \Delta$ is required.

fermions f_{12} and f_{34} , we can assume the same way to empty the occupation of the regular fermion f_{23} associated with the fused MZMs γ_2 and γ_3 , by introducing an additional tunnel-coupled side QD (electron-mediating QD) and modulating the dot energy level $\tilde{\epsilon}_D$ in resonance with the Majorana energy ϵ_M , while the electron-mediating QD is tunnel coupled to an outside reservoir with the Fermi level lower than $\tilde{\epsilon}_D$. This can ensure $n_{23} = 0$. Starting with it, perform the measurement of steady-state current power spectrum, one can obtain the single peak height $h_A^{(0)}$ at $\omega = 2\Omega_A$. To obtain $h_N^{(0)}$, after ensuring $n_{23} = 0$ as explained above, one can input an electron from the reservoir into an occupation of the regular fermion f_{23} through the electron-mediating QD by increasing the Fermi level of the reservoir above $\tilde{\epsilon}_D$. Then starting with $n_{23} = 1$ and performing the steady-state spectrum measurement, one can obtain the single peak height $h_N^{(0)}$ at $\omega = 2\Omega_A$. Finally, we remark that, to realize the definite occupation result $n_{23} = 0$ or 1 as described above, the Andreev process should be suppressed. This requires a weak coupling of the regular fermion f_{23} to the electron-mediating QD, i.e., with the coupling strength much smaller than ϵ_M and $\tilde{\epsilon}_D$.

VI. SUMMARY AND DISCUSSION

For the purpose of demonstrating the nontrivial fusion of MZMs, which requires a preparation of initial state of

Majorana pairs with definite fermion parity and moving the MZMs (to be fused) together from distant locations, we performed simulations of moving a MZM in a TSC quantum wire. We simulated the gradual moving of a MZM through modulations of multiple segments from nontopological to topological transitions and displayed interesting behaviors of the nonadiabatic transition. We also analyzed in detail the result of intrinsic fermion-parity breaking of MZMs by identifying its origin of being induced/mediated by the nonadiabatic transition to high-energy excited states and analyzed its consequence to the result of nontrivial fusion of two MZMs. Moreover and most importantly, we developed a scheme to simultaneously infer both the degree of fermion parity breaking and nonadiabatic transition probability to excited states, based on the characteristic spectrum of measurement current, by using the locations and heights of two characteristic peaks. We are not aware of similar studies in the literature, and this probing protocol should therefore be of great interest to the Majorana community.

About the deviation from the statistics of outcomes of nontrivial fusion, owing to fermion parity breaking during moving the MZM in each single TSC quantum wire, we may add some more discussions as follows. In our simulation of moving the Majorana mode, we only consider two Majorana modes in a single wire (e.g., γ_1 and γ_2). Associated with the fermion parity breaking, the state transfer sequence is $|0_{12}\rangle \rightarrow |1_n\rangle \rightarrow |1_{12}\rangle$. Here, to be more clear, we use the number-state representation. In the first process, a Cooper pair is split into two electrons, with one electron being excited to the gap-above quasiparticle state $|1_n\rangle$, while another electron is submerged into the sea of background normal electrons. In the second process, the electron is transitioned from the quasiparticle state to the subgap (near zero-energy) state. As a result, the occupation of the subgap state of a single wire (e.g., the left wire) is $\alpha_L|0_{12}\rangle + \beta_L|1_{12}\rangle$. For the two wires, the total state is a product of the two wire states, as shown by Eq. (5). Then owing to the appearance of $|1_{12}\rangle$ and $|1_{34}\rangle$ (i.e., violation of the fermion parity of each single wire), the quantum average of the parity operator $P_{23} = i\gamma_2\gamma_3$ becomes nonzero $\langle P_{23} \rangle \neq 0$, which differs from the result $\langle P_{23} \rangle = 0$, i.e., the prediction for the statistics of the nontrivial fusion outcomes [13].

We notice that, in Ref. [22], the 4-MZM qubit is considered for possible qubit loss (escape from the subspace of qubit states), bit-flip error, and phase-flip error, mediated by the nonadiabatic transition (through the excitation spectrum), owing to moving the Majorana mode and/or noise-caused fluctuations. For the bit flip between the logic states $|0_{12}0_{34}\rangle$ and $|1_{12}1_{34}\rangle$, an effective coupling between γ_2 and γ_3 may be explored to describe it, using the coupling Hamiltonian $H' = i\epsilon_{23}\gamma_2\gamma_3$, which is like the parity operator $P_{23} = i\gamma_2\gamma_3$. In Ref. [22], the qubit flip error $|0_{12}0_{34}\rangle \rightarrow |1_{12}1_{34}\rangle$, mediated by the nonadiabatic transition through the gap-above excited states, experiences the following state transfer sequence: $|0_{12}0_{34}\rangle|0_n\rangle \rightarrow |1_{12}0_{34}\rangle|1_n\rangle \rightarrow |1_{12}1_{34}\rangle|0_n\rangle$, where $|1_n\rangle$ and $|0_n\rangle$ correspond to the excited state $|\psi_{+E_n}\rangle$ occupied and unoccupied. The underlying physics of the first process is associated with splitting of a Cooper pair, while the second process is a usual quantum transition from $|\psi_{+E_n}\rangle$ to $|\psi_{+E_0}\rangle$.

The essential difference between the result of bit-flip error in Ref. [22] and ours is, for the flip error of the 4-MZM qubit $|0_{12}0_{34}\rangle \rightarrow |1_{12}1_{34}\rangle$, the total fermion parity is conserved; while in our case, the result $|0_{12}\rangle \rightarrow |1_{12}\rangle$ indicates a violation of the fermion parity, in a *closed* single wire. In our opinion, the latter effect is of more interest. In practice, this effect can be measured along the analysis in this paper. To restrict the nonadiabatic transition occurring in each single wire, the two wires should be interrupted at the center by a gate-controlled

potential barrier [see Fig. 1(a)], before the two MZMs (to be fused) are moved close to each other (during the moving process). The fusion can be realized by lowering the barrier after the two MZMs are moved close to each other.

ACKNOWLEDGMENTS

This work was supported by the NNSF of China (Grants No. 11974011 and No. 11904261).

-
- [1] A. Y. Kitaev, Unpaired Majorana fermions in quantum wires, *Phys. Usp.* **44**, 131 (2001).
- [2] A. Y. Kitaev, Fault-tolerant quantum computation by anyons, *Ann. Phys.* **303**, 2 (2003).
- [3] C. Nayak, S. H. Simon, A. Stern, M. Freedman, and S. D. Sarma, Non-Abelian anyons and topological quantum computation, *Rev. Mod. Phys.* **80**, 1083 (2008).
- [4] B. M. Terhal, Quantum error correction for quantum memories, *Rev. Mod. Phys.* **87**, 307 (2015).
- [5] S. D. Sarma, M. Freedman, and C. Nayak, Majorana zero modes and topological quantum computation, *npj Quantum Inf.* **1**, 15001 (2015).
- [6] Y. Oreg and F. von Oppen, Majorana zero modes in networks of Cooper-pair boxes: Topologically ordered states and topological quantum computation, *Annu. Rev. Condens. Matter Phys.* **11**, 397 (2020).
- [7] J. Alicea, Y. Oreg, G. Refael, F. von Oppen, and M. Fisher, Non-Abelian statistics and topological quantum information processing in 1D wire networks, *Nat. Phys.* **7**, 412 (2011).
- [8] B. I. Halperin, Y. Oreg, A. Stern, G. Refael, J. Alicea, and F. von Oppen, Adiabatic manipulations of Majorana fermions in a three-dimensional network of quantum wires, *Phys. Rev. B* **85**, 144501 (2012).
- [9] F. Harper, A. Pushp, and R. Roy, Majorana braiding in realistic nanowire Y-junctions and tuning forks, *Phys. Rev. Res.* **1**, 033207 (2019).
- [10] C. Tutschku, R. W. Reinthaler, C. Lei, A. H. MacDonald, and E. M. Hankiewicz, Majorana-based quantum computing in nanowire devices, *Phys. Rev. B* **102**, 125407 (2020).
- [11] T. Sanno, S. Miyazaki, T. Mizushima, and S. Fujimoto, *Ab initio* simulation of non-Abelian braiding statistics in topological superconductors, *Phys. Rev. B* **103**, 054504 (2021).
- [12] D. Aasen, M. Hell, R. Mishmash, A. Higginbotham, J. Danon, M. Leijnse, T. Jespersen, J. Folk, C. Marcus, K. Flensberg *et al.*, Milestones toward Majorana-based quantum computing, *Phys. Rev. X* **6**, 031016 (2016).
- [13] C. W. J. Beenakker, Search for non-Abelian Majorana braiding statistics in superconductors, *SciPost Phys. Lect. Notes* **1**, 15 (2020).
- [14] T. Zhou, M. C. Dartiailh, K. Sardashti, J. E. Han, A. Matos-Abiague, J. Shabani, and I. Žutić, Fusion of Majorana bound states with mini-gate control in two-dimensional systems, *Nat. Commun.* **13**, 1738 (2022).
- [15] J. Bai, Q. Wang, L. Xu, W. Feng, and X.-Q. Li, Probing the non-Abelian fusion of a pair of Majorana zero modes, *Phys. Rev. B* **109**, 085403 (2024).
- [16] R. S. Souto and M. Leijnse, Fusion rules in a Majorana single-charge transistor, *SciPost Phys.* **12**, 161 (2022).
- [17] T. Zhou, M. C. Dartiailh, W. Mayer, J. E. Han, A. Matos-Abiague, J. Shabani, and I. Žutić, Phase control of Majorana bound states in a topological X junction, *Phys. Rev. Lett.* **124**, 137001 (2020).
- [18] C.-X. Liu, H. Pan, F. Setiawan, M. Wimmer, and J. D. Sau, Fusion protocol for Majorana modes in coupled quantum dots, *Phys. Rev. B* **108**, 085437 (2023).
- [19] D. J. Clarke, J. D. Sau, and S. Tewari, Majorana fermion exchange in quasi-one-dimensional networks, *Phys. Rev. B* **84**, 035120 (2011).
- [20] M. Sekania, S. Plugge, M. Greiter, R. Thomale, and P. Schmitteckert, Braiding errors in interacting Majorana quantum wires, *Phys. Rev. B* **96**, 094307 (2017).
- [21] B. Bauer, T. Karzig, R. V. Mishmash, A. E. Antipov, and J. Alicea, Dynamics of Majorana-based qubits operated with an array of tunable gates, *SciPost Phys.* **5**, 004 (2018).
- [22] A. Conlon, D. Pellegrino, J. K. Slingerland, S. Dooley, and G. Kells, Error generation and propagation in Majorana-based topological qubits, *Phys. Rev. B* **100**, 134307 (2019).
- [23] M. Narożniak, M. C. Dartiailh, J. P. Dowling, J. Shabani, and T. Byrnes, Quantum gates for Majoranas zero modes in topological superconductors in one-dimensional geometry, *Phys. Rev. B* **103**, 205429 (2021).
- [24] M. Cheng, V. Galitski, and S. Das Sarma, Nonadiabatic effects in the braiding of non-Abelian anyons in topological superconductors, *Phys. Rev. B* **84**, 104529 (2011).
- [25] T. Karzig, G. Refael, and F. von Oppen, Boosting Majorana zero modes, *Phys. Rev. X* **3**, 041017 (2013).
- [26] M. S. Scheurer and A. Shnirman, Nonadiabatic processes in Majorana qubit systems, *Phys. Rev. B* **88**, 064515 (2013).
- [27] T. Karzig, A. Rahmani, F. von Oppen, and G. Refael, Optimal control of Majorana zero modes, *Phys. Rev. B* **91**, 201404(R) (2015).
- [28] A. Rahmani, B. Seradjeh, and M. Franz, Optimal diabatic dynamics of Majorana-based quantum gates, *Phys. Rev. B* **96**, 075158 (2017).
- [29] A. Nag and J. D. Sau, Diabatic errors in Majorana braiding with bosonic bath, *Phys. Rev. B* **100**, 014511 (2019).
- [30] B. P. Truong, K. Agarwal, and T. Pereg-Barnea, Optimizing the transport of Majorana zero modes in one-dimensional topological superconductors, *Phys. Rev. B* **107**, 104516 (2023).
- [31] L. Xu and X.-Q. Li, Transport probe of the nonadiabatic transition caused by moving Majorana zero modes, *Phys. Rev. B* **105**, 245410 (2022).

- [32] E. Prada, P. San-Jose, and R. Aguado, Transport spectroscopy of NS nanowire junctions with Majorana fermions, *Phys. Rev. B* **86**, 180503(R) (2012).
- [33] S. Das Sarma, J. D. Sau, and T. D. Stanescu, Splitting of the zero-bias conductance peak as smoking gun evidence for the existence of the Majorana mode in a superconductor-semiconductor nanowire, *Phys. Rev. B* **86**, 220506(R) (2012).
- [34] D. Rainis, L. Trifunovic, J. Klinovaja, and D. Loss, Towards a realistic transport modeling in a superconducting nanowire with Majorana fermions, *Phys. Rev. B* **87**, 024515 (2013).
- [35] A. N. Korotkov, Output spectrum of a detector measuring quantum oscillations, *Phys. Rev. B* **63**, 085312 (2001).
- [36] A. A. Zhukov, D. S. Shapiro, W. V. Pogosov, and Y. E. Lozovik, Dynamics of a mesoscopic qubit ensemble coupled to a cavity: Role of collective dark states, *Phys. Rev. A* **96**, 033804 (2017).
- [37] X. Q. Li, P. Cui, and Y. J. Yan, Spontaneous relaxation of a charge qubit under electrical measurement, *Phys. Rev. Lett.* **94**, 066803 (2005).
- [38] J. F. Steiner and F. von Oppen, Readout of Majorana qubits, *Phys. Rev. Res.* **2**, 033255 (2020).